Calibrating calving parameterizations using graph neural network emulators: Application to Helheim Glacier, East Greenland

Younghyun Koo[1], Gong Cheng[2], Mathieu Morlighem[2], and Maryam Rahnemoonfar[1,3]

[1]Department of Computer Science and Engineering, Lehigh University, 27 Memorial Dr W, Bethlehem, PA 18015, USA
[2]Department of Earth Sciences, Dartmouth College, Hanover, NH 03755, USA
[3]Department of Civil and Environmental Engineering, Lehigh University, 27 Memorial Dr W, Bethlehem, PA 18015, USA
Correspondence: Maryam Rahnemoonfar (maryam@lehigh.edu)

Abstract. Calving is responsible for the retreat, acceleration, and thinning of numerous tidewater glaciers in Greenland. An accurate representation of this process in ice sheet numerical models is critical in order to better predict the future response of the ice sheet to climate change. While traditional numerical models have succeeded in simulating ice dynamics and calving under specific parameterized conditions, the computational demand of these models makes it difficult to efficiently fine-tune

5 these parameterizations, adding to the overall uncertainty in future sea level rise. Here, we develop various standard Graph Neural Network (GNN) architectures, including graph convolutional network (GCN), graph attention network (GAT), and equivariant graph convolutional network (EGCN), to construct surrogate models of finite-element simulations from the Ice-sheet and Sea-level System Model. GNNs are particularly well suited for this problem as they naturally capture the representation of unstructured meshes used by finite-element models. When these GNNs are trained with the simulation results of Helheim Glacier,

10 Greenland, for different calving stress thresholds, they successfully reproduce the evolution of ice velocity, ice thickness, and ice front migration between 2007 and 2020. GNNs show better fidelity than convolutional neural networks (CNN) particularly near the boundaries of fast ice streams, and EGCN outperforms the others by preserving the equivariance of graph structures. By using the GPU-based GNN emulators, which are 260-560 times faster than the numerical simulations, we determine the optimal range of the calving threshold that minimizes the misfit between the modeled and observed ice fronts.

1 Introduction

15 Over the past three decades, the Greenland ice sheet has experienced an average annual loss of 170 Gt of ice, resulting in a global mean sea level rise exceeding 15 mm (Otosaka et al., 2023). This trend of mass loss has intensified in recent years. Between 1990 and 2000, the annual mass loss hovered around 40 Gt/year, but in the 2010s, it surged to approximately 280 Gt/year (Otosaka et al., 2023; Mouginot et al., 2019). This escalating mass loss can be attributed to two primary processes: (1) the

20 change in surface mass balance driven by enhanced surface melt and (2) calving and submarine melting of marine-terminating glaciers, commonly referred to as frontal ablation (King et al., 2020; Choi et al., 2021). In specific regions and seasons, ice discharge may be responsible for more than 50% of the total mass loss. (Mouginot et al., 2019; King et al., 2020; Choi et al., 2021; Aschwanden et al., 2019).

Enhanced calving significantly impacts ice dynamics, often resulting in ice flow acceleration and subsequent thinning (Bondzio
25 et al., 2017; Cheng et al., 2022; Lippert et al., 2024). Given that calving is sensitive to climate conditions (Greene et al., 2024b;
Wood et al., 2021), it is important to understand how future calving rates would impact ice sheet mass balance, and sea-level rise
(Choi et al., 2021). Numerous studies have utilized ice sheet numerical models to explore the applicability of various calving
laws to Greenland and Antarctic ice sheets, aiming to identify optimal parameterizations (Wilner et al., 2023; Choi et al., 2018).
According to Choi et al. (2018), the von Mises calving law (VM) (Morlighem et al., 2016) best replicates observed terminus
30 positions of nine outlet glaciers in Greenland compared to other existing laws. However, the optimal parameters for VM may
vary significantly among different glaciers across both Greenland and Antarctica (Wilner et al., 2023; Choi et al., 2018).

Although numerical models can provide reliable solutions for ice flow when ice extent is kept constant, capturing the precise
impacts of spatiotemporally varying calving rates on terminus migration and ice flow in numerical models remains challenging.
Additionally, assimilating remote sensing observations into numerical models, required to infer certain model parameters, is both
35 complex to implement and computationally intensive (Choi et al., 2023). Furthermore, the integration of calving as boundary
conditions in the numerical models introduces significant complexity since calving directly alters the ice geometry and model
domain during simulations. Consequently, identifying the optimal calving parameterizations consistent with observations is
difficult and time-consuming, thereby limiting our ability to project the future mass balance of ice sheets under various parameter
settings (Choi et al., 2018; Edwards et al., 2021; Morlighem et al., 2020).

40 To address the computational demands of numerical models, various approaches have emerged relying on faster machine
learning models in lieu of ice sheet numerical models. While traditional numerical models often necessitate high-performance
computing clusters to solve partial differential equations (PDEs) on central processing units (CPUs), machine learning emulators
offer the advantage of operating on lighter computational resources, leveraging the parallel processing capabilities of graphic
processing units (GPUs). In terms of model architecture, prior research predominantly relied on a Convolutional Neural Network
45 (CNN) for emulating ice sheet dynamics (Jouvet et al., 2022; Jouvet and Cordonnier, 2023). However, since CNNs are tailored
for regular Euclidean grid structures, such as images, they may not be the optimal choice for replicating the unstructured meshes
characteristic of finite-element-based numerical models. In particular, the regular grid structure of CNN may lead to a loss of
several advantages inherent in unstructured meshes, such as efficient allocation of computational resources and finer resolution
in fast ice regions.

50 In recent years, Graph Neural Networks (GNNs) have gained attention as a viable alternative to CNNs, particularly for
handling irregular non-Euclidean data structures such as molecular structures, point clouds, social networks, and natural language
(Zhang et al., 2019). Unlike CNNs, GNNs are adaptable to any type of data structure organized as graphs, comprising *nodes* (i.e.,
data points) and *edges* (i.e., the connections between nodes). GNNs make predictions by utilizing pairwise message-passing
between nodes, wherein information exchange occurs, updating individual node features through interactions with connected
55 nodes. Inspired by the resemblance of the mesh structure in finite-element analysis to a graph structure, numerous studies have
investigated the use of emulators of finite-element numerical simulations using GNNs (Fu et al., 2023; Shivaditya et al., 2022;
Black and Najafi, 2022; Perera et al., 2022; Salehi and Giannacopoulos, 2022; Maurizi et al., 2022; Jiang and Chen, 2023).

In this study, we develop GNN emulators of an ice sheet numerical model to speed up the analysis of calving parameterization effects on ice dynamics. Our focus is on Helheim Glacier, in Southeast Greenland, chosen as the target site for training and

60   evaluating our GNN emulators (Fig. 1a). Helheim Glacier is one of the largest outlet glacier in Greenland and it has been shown that its ice velocity is closely correlated to the position of its terminus (Cheng et al., 2022). Despite considerable advancements over the past decades, the mechanisms governing Helheim Glacier's ice front position remain elusive (Bevan et al., 2015; Miles et al., 2016; Cheng et al., 2022). A key contributing factor to this knowledge gap is the computational intensity of numerical models incorporating calving, impeding the fine-tuning of calving parameters to accurately reflect observations. Here, we train

65   GNN models using simulation data derived from a traditional numerical model and evaluate their fidelity and computational efficiency in modeling the ice dynamics and calving of Helheim Glacier.

The remainder of the paper is structured as follows. Section 2 provides a comprehensive review of relevant literature about calving parameterization in ice sheet models, the use of GNNs as emulators for finite-element models, and other machine-learning emulators employed in ice sheet modeling. In Section 3, we describe the training data collected from numerical

70   simulations, while Section 4 outlines the specifics of GNN architectures alongside a baseline CNN model. Section 5 presents the accuracy and computational efficiency of these models in replicating the dynamics of Helheim Glacier. Finally, we demonstrate the utility of GNN emulators in optimizing calving parameterization.

2   Background

2.1   von Mises calving law

75   In the von Mises calving law, the calving rate, c, is assumed to be proportional to both the tensile stress and the magnitude of ice velocity, formulated as follows (Morlighem et al., 2016):

$$c = ||\boldsymbol{v}|| \frac{\tilde{\sigma}}{\sigma_{\max}} \tag{1}$$

where $\tilde{\sigma}$ is a scalar quantity representing the effective tensile stress of the ice, $\sigma_{\max}$ is a stress threshold that needs to be calibrated on a glacier-by-glacier basis, and $\boldsymbol{v}$ is the ice flow velocity at the ice front. The moving velocity of the ice front is then determined

80   from the calving rate c using the following equation (Morlighem et al., 2016):

$$\boldsymbol{v}_f = \boldsymbol{v} - (c + \dot{M})\boldsymbol{n} \tag{2}$$

where $\boldsymbol{v}_f$ is the ice front velocity, $\dot{M}$ is the melting rate on the calving front, and $\boldsymbol{n}$ is a unit normal vector pointing outward from the ice domain. In the Ice-sheet and Sea-level System Model (ISSM), the numerical ice sheet model we use in this study, moving boundaries of ice sheets are represented implicitly using the level set method (Osher and Sethian, 1988; Bondzio et al.,

85   2016; Morlighem et al., 2016). The level set method defines a scalar field $\varphi(\boldsymbol{x}, t)$ that is negative in the location of $\boldsymbol{x}$ that are ice covered at time t, positive where there is no ice, and the zero contour of φ defines the ice boundary.

In VM, $\sigma_{\max}$ is the only parameter that needs to be calibrated (Morlighem et al., 2016). A lower value of $\sigma_{\max}$ correlates with easier ice calving and consequently, a larger calving rate. According to Morlighem et al. (2016), $\sigma_{\max}$ is consistent with the
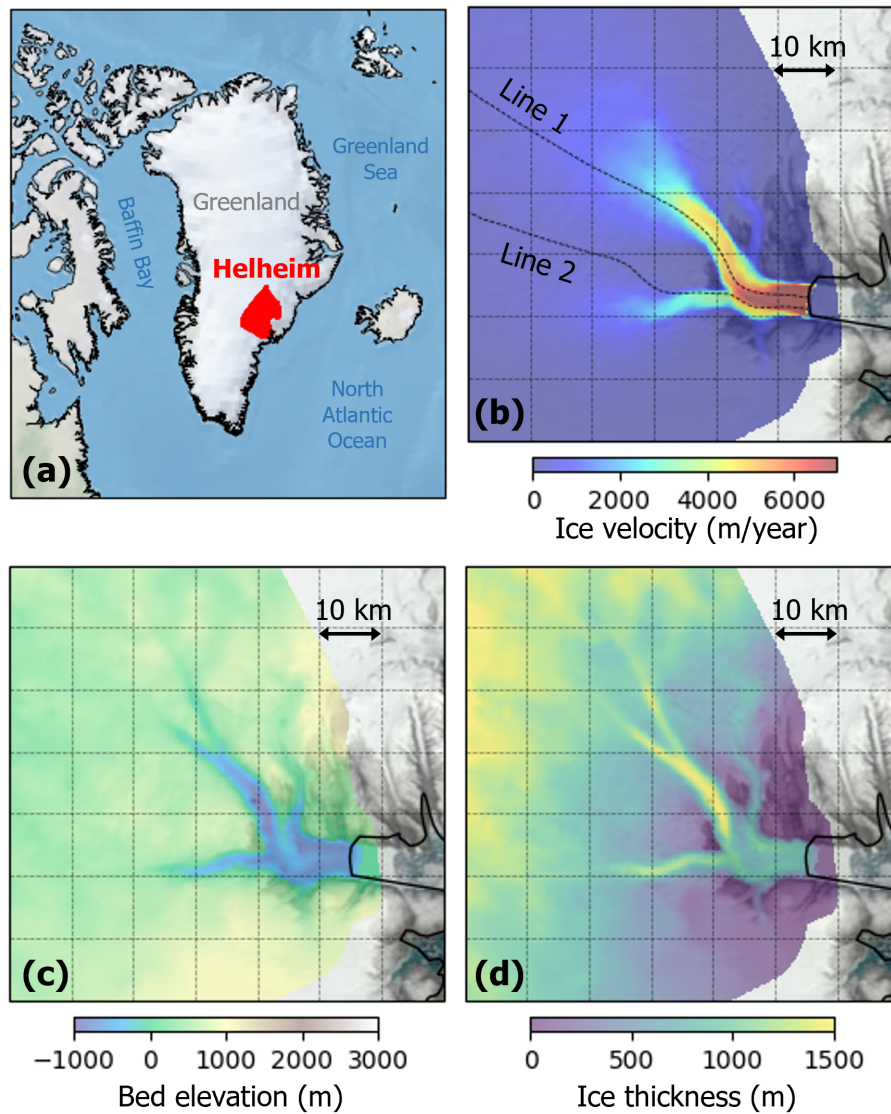
Figure 1. (a) Location of Helheim Glacier, Greenland; (b) ice velocity, (c) bed elevation, and (d) ice thickness near the calving front of Helheim glacier in 2007. The background image is the MODIS true color image from June 20, 2023.

range of ice tensile strength, which is typically around 1 MPa, but may be as low as 0.7 MPa or exceed 3 MPa. However, since

90 σ_{max} can vary spatially, and even temporally, among different Greenlandic glaciers (Choi et al., 2018; Downs et al., 2023), finely calibrating σ_{max} is the key for accurately modeling ice dynamics.

2.2 Graph neural networks for finite-element analysis

GNNs have been broadly used to emulate finite-element numerical models due to the similarities between a computational mesh and graphs. Perera et al. (2022) developed a GNN framework to simulate fracture and stress evolution in brittle materials, training

95 their model with data generated from a finite-element method fracture solver. Similarly, Shivaditya et al. (2022) proposed a GNN surrogate model for finite-element simulations of metal forging processes, demonstrating superior performance compared to other machine learning models and achieving a tenfold reduction in processing time. Salehi and Giannacopoulos (2022) also developed PhysGNN, a GNN framework tailored for simulating soft tissue deformation, and Maurizi et al. (2022) utilized GNNs to predict stress, strain, and deformation across various material systems, including fiber and stratified composites, and lattice

100 metamaterials. Fu et al. (2023) proposed a boundary-oriented graph embedding (BOGE) approach within the GNN framework for solving finite-element cantilever beam problems, incorporating both boundary elements and local neighbor elements. Jiang and Chen (2023) introduced a novel graph attribute representation for triangular meshes in finite-element von Mises stress problems, effectively capturing geometry and boundary conditions to mitigate over-smoothing issues associated with deep GNNs. Black and Najafi (2022) introduced a multi-fidelity GNN for the cantilever beam problem, leveraging low-fidelity

105 projections to inform high-fidelity modeling across arbitrary subdomains of subgraphs. However, despite the prevalence of finite-element analysis in ice sheet modeling (Larour et al., 2012; dos Santos et al., 2021; Gagliardini et al., 2013), to the best of our knowledge, GNNs have yet to be adopted for simulating ice flow and calving modeling.

2.3 Machine learning emulator for ice sheet modeling

Machine learning techniques, predominantly CNNs, have been extensively employed as statistical emulators for numerical ice

110 sheet models (Jouvet et al., 2022; Jouvet and Cordonnier, 2023; Jouvet, 2023; Verjans and Robel, 2024). For instance, the CNN of the Instructed Glacier Model (IGM) (Jouvet et al., 2022) reproduced the ice dynamics from the Parallel Ice Sheet Model (Winkelmann et al., 2011, PISM) and CfsFlow models (Jouvet et al., 2008). Jouvet (2023) extended this CNN emulator to address inversion problems, inferring optimal ice thickness distribution, ice flow velocity, and ice surface elevation to match both a Stokes model and observational data. Another CNN emulator introduced by Jouvet and Cordonnier (2023) employed a

115 physics-informed loss function to minimize the energy associated with ice-flow equations during training. Verjans and Robel (2024) developed a CNN-based emulator to model subglacial hydrology in several Greenland glaciers. Despite the computational advantages of CNN-based emulators over numerical models, CNN cannot fully represent finite-element ice sheet modeling because it relies on regular grids (Zhang et al., 2019). Instead of CNN, He et al. (2023) employed a neural operator architecture to replace finite-element modeling of ice velocity based on Shelfy Stream Approximation (SSA). By using a hybrid approach

120 integrating neural operators with finite-element methods, they retain a classical finite-element discretization for the evolution of the ice thickness. While prior studies have primarily focused on emulators for general ice flow problems, no studies have

focused on calving dynamics using machine learning emulators. Given the GNN's capacity to account for dynamic interactions between nodes and edges (Satorras et al., 2022), it emerges as a promising tool for predicting the dynamic behavior of ice, including ice front migration.

125 3   Training Data and Observations

3.1   Ice Sheet numerical simulation

To generate training datasets for the GNN emulators, we conduct transient simulations of ice dynamics and calving of Helheim Glacier between 2007 and 2020, using the Ice-sheet and Sea-level System Model (ISSM Larour et al., 2012). The Shelfy-Stream Approximation (SSA MacAyeal, 1989) is used for describing ice flow. The SSA, which assumes depth-independent horizontal
130   velocity and negligible vertical shear stresses, is appropriate for fast-flowing glaciers controlled by basal sliding such as Helheim Glacier (Cheng et al., 2022; Choi et al., 2018).

The model setup is identical to the one described in Cheng et al. (2022). A two-dimensional unstructured mesh is constructed with a spatial resolution ranging from 100 m in the fast-flowing ice front to 1,500 m in the inland domain, ultimately comprising 46,434 elements and 23,466 vertices (nodes). The transient simulations run forward in time with a time step of 1.825 days (0.005
135   years), and we output the state of the model every 10 time steps (∼18 days). Consequently, each single transient simulation generates a total of 261 results between 2007 and 2020. Basal friction is calibrated using the surface velocities from satellite interferometry (Mouginot et al., 2017, 2019) (Fig. 1b); bed topography and the initial ice thickness are from BedMachine Greenland v6 (Morlighem et al., 2017) (Fig. 1c and 1d); surface mass balance (SMB) is from the Regional Atmosphere Model (Tedesco and Fettweis, 2020); the ocean thermal forcing is from Wood et al. (2021). The melting rate at the calving front (i.e.,
140    $\dot{M}$ in Eq. 2) is parameterized based on Rignot et al. (2016). To examine the sensitivity of ice dynamics to σ_{max} of the VM calving law, we run transient solutions for 9 different σ_{max} values (i.e., 0.70, 0.75, 0.80, 0.85, 0.90, 0.95, 1.00, 1.05, and 1.10 MPa) based on the values proposed by Choi et al. (2018).

The ISSM simulations provide the solutions of ice velocity, ice thickness, and a mask of ice-covered region every 10 time steps. We convert the triangular mesh from ISSM into a data structure that aligns with the input and output requirements of deep
145   learning architectures. Specifically, for GNN architectures, we convert the meshes into graph nodes and edges by extracting adjacent matrices that represent the connectivity between nodes. In a triangular mesh, each element consists of three nodes that are interconnected by edges (Fig. 2). Using the nodes and elements of the mesh ensures that the resolution of this graph matches exactly with the finite-element mesh used in ISSM simulations. However, for the CNN architecture that requires regular grid data structures, we interpolate the ISSM mesh into a 200 m×200 m grid using a bilinear interpolation.

150 3.2   Observations

To determine the best σ_{max} that aligns with real observations, we collect remote-sensing derived terminus positions and ice velocities for the same periods as the numerical simulations (2007-2020). First, we use surface ice velocities with a spatial

resolution of 150 m (Mouginot et al., 2017, 2019), which have a precision better than 20 m/year (Mouginot et al., 2017). Second, we use a time series of calving front positions of Helheim Glacier from Greene et al. (2024a). During the targeted time frame
155   from 2007 to 2020, we use monthly averaged ice front positions, yielding a total of 156 distinct ice front positions for analysis.

4   Method

Ice sheet modeling can be regarded as a node-regression problem within graph structures, where the output features of individual nodes are derived from the input features of nodes. The unstructured meshes of ISSM can be represented as graph structures, with node connectivity expressed via adjacency matrices. Based on the graph structures of the ISSM meshes, we develop three
160   GNN architectures: graph convolutional network (GCN), graph attention network (GAT), and equivariant graph convolutional network (EGCN). Typical GNN architectures update graph nodes iteratively through message-passing processes between neighboring nodes, and the way to achieve this message-passing determines the specific type of GNN architecture. For the undirected graph $\mathcal{G} = (\mathcal{V}, \mathcal{E})$ with N nodes $v_i \in \mathcal{V}$, edges $(v_i, v_j) \in \mathcal{E}$, and an adjacency matrix $A \in \mathbb{R}^{N \times N}$, lth GNN layer receives a set of node features $\mathbf{h}^{(l)} = \{h_1^{(l)}, h_2^{(l)}, ..., h_N^{(l)}\}, h_i^{(l)} \in \mathbb{R}^{F_l}$, as the input and produces a new set of node features,
165    $\mathbf{h}^{(l+1)} = \{h_1^{(l+1)}, h_2^{(l+1)}, ..., h_N^{(l+1)}\}, h_i^{(l+1)} \in \mathbb{R}^{F_{l+1}}$, for the next $l+1$th layer. F_l and F_{l+1} is the number of features in each node at lth layer and $l+1$ layer, respectively. The GCN, GAT, and EGCN operate on graph structures but use different message-passing approaches in updating $\mathbf{h}^{(l+1)}$ from $\mathbf{h}^{(l)}$. By comparing three representative GNN architectures, we evaluate what approach is more effective in replicating ice sheet dynamics and calving from the ISSM simulations.

4.1   Graph Convolutional Network

170   First, we employ a GCN proposed by Kipf and Welling (2017). We design a GCN with one input layer, five graph convolutional hidden layers, and one output layer (Fig. 2). The number of hidden layers is determined after conducting trial and error experiments with several options: we tested 1, 2, 5, and 10 hidden layers, and 5 hidden layers showed the best accuracy. The graph convolutional hidden layers are inspired by the localized first-order approximation of spectral graph convolutions on graph-structured data (Kipf and Welling, 2017). For each graph convolutional layer, the number of features is set to 128. Similar
175   to the hidden layers, the number of hidden features was determined from trial and error with 4 options: 32, 64, 128, and 256. The weights of graph convolutional layers are updated via the layer-wise propagation rule as follows:

$$h_i^{(l+1)} = \sigma \left(\sum_{j \in \mathcal{N}(i)} \frac{1}{c_{ij}} \mathbf{W}^{(l)} h_j^{(l)} \right) \tag{3}$$

where $\mathcal{N}(i)$ is the set of neighbors of node i, c_{ij} is an appropriately chosen normalization constant for the edge (v_i, v_j) defined as the product of the square root of node degrees (i.e., $c_{ij} = \sqrt{|\mathcal{N}(j)|}\sqrt{|\mathcal{N}(i)|}$), and $\mathbf{W}^{(l)} \in \mathbb{R}^{F_{l+1} \times F_l}$. $\mathbf{W}^{(l)}$ is a layer-specific
180   trainable weight matrix ($\mathbf{W}^{(l)} \in \mathbb{R}^{F_{l+1} \times F_l}$), and $\sigma(\cdot)$ is an activation function; we use the Leaky ReLU activation function of 0.01 negative slope in this study.

[EGUsphere Preprint repository logo]
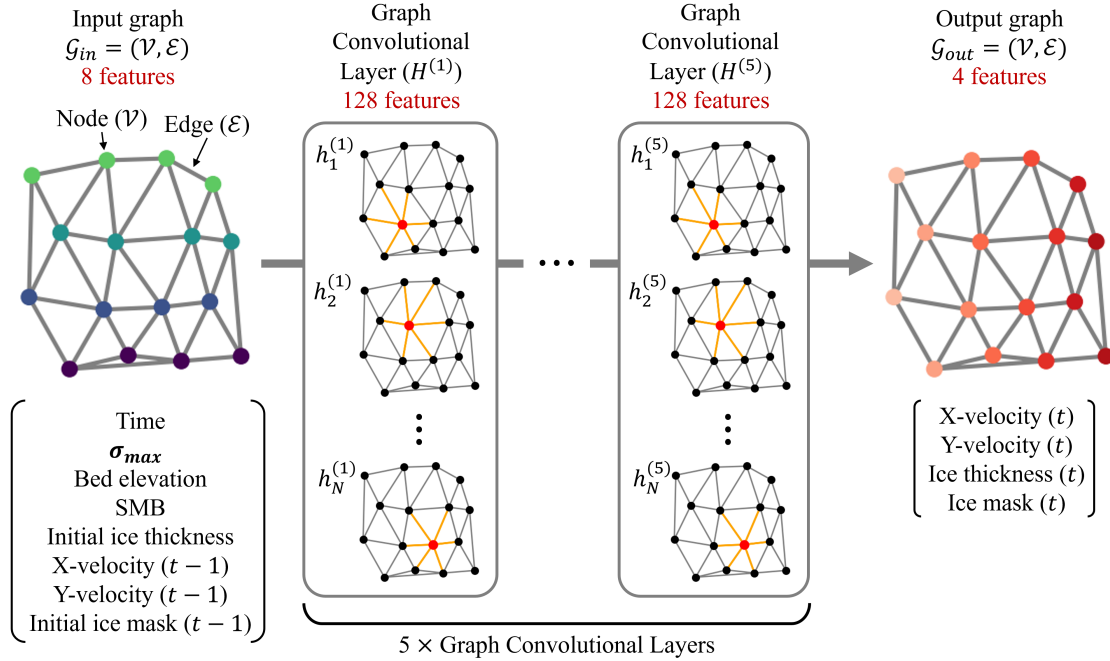
Figure 2. Schematic illustration of GCN architectures. All graph convolutional layers are replaced with graph attention layers for GAT, equivariant graph convolutional layers for EGCN, and 3×3 convolutional layers for FCN.

4.2 Graph Attention Network

Since the original GCN filters merely depend on graph structures and node connectivity (Eq. 3), a model trained with a certain graph structure can have limitations in general applicability to different graph structures. The GAT is proposed to address such shortcomings by adding masked self-attention layers (Veličković et al., 2018). This architecture assigns different weights to different nodes in a neighborhood by stacking self-attention layers (Fig. 3a), which can allow better generalizability for different ice conditions or topographies. The propagation process in graph attention layers can be expressed by the following equation (Veličković et al., 2018):

$$h_i^{(l+1)} = \sigma \left(\sum_{j \in \mathcal{N}(i)} \alpha_{ij}^{(l)} \mathbf{W}^{(l)} h_j^{(l)} \right) \tag{4}$$

where $\alpha^{(l)}$ is the attention score between node i and node j defined as follows:

$$\alpha_{ij}^{(l)} = \text{softmax}_j \left(e_{ij}^{(l)} \right) = \frac{\exp(e_{ij}^{(l)})}{\sum_{k \in \mathcal{N}(i)} \exp(e_{ik}^{(l)})}$$
$$e_{ij}^{(l)} = a \left(\mathbf{W}^{(l)} h_i^{(l)}, \mathbf{W}^{(l)} h_j^{(l)} \right) \tag{5}$$

where $a : \mathbb{R}^{F_{l+1}} \times \mathbb{R}^{F_{l+1}} \to \mathbb{R}$ is a self-attention mechanism to compute attention coefficient $e_{ij}^{(l)}$. This attention mechanism a is a single-layer feedforward neural network parameterized by a weight vector $\mathbf{a} \in \mathbb{R}^{2F_{l+1}}$, normalized by LeakyReLU function afterward. The graph structure is applied to this attention mechanism by computing $e_{ij}^{(l)}$ for only nodes $j \in \mathcal{N}(i)$ where $\mathcal{N}(i)$ is set of neighbors of node i. Thus, the attention score $\alpha^{(l)}$ can be expressed as follows:

$$\alpha_{ij}^{(l)} = \frac{\exp\left(\text{LeakyReLU}(\mathbf{a}^T[\mathbf{W}^{(l)}h_i^{(l)}||\mathbf{W}^{(l)}h_j^{(l)}])\right)}{\sum_{k \in \mathcal{N}(i)} \exp\left(\text{LeakyReLU}(\mathbf{a}^T[\mathbf{W}^{(l)}h_i^{(l)}||\mathbf{W}^{(l)}h_k^{(l)}])\right)} \tag{6}$$

where $\cdot^T$ denotes transpose operator and $||$ is the concatenation operation. We execute three independent attention mechanisms of Equation 4 and average them for the final graph attention layer (Veličković et al., 2018). Similar to the GCN, the GAT consists of one input layer, five graph attention hidden layers with 128 features, and one output layer (Fig. 2).

4.3 Equivariant Graph Convolutional Network

Another graph neural network we develop is EGCN, which is designed to conserve equivariance to rotations, translations, reflections, and permutations in a graph structure (Satorras et al., 2022) (Fig. 3b). Since our emulator is intended to predict ice front migration, we anticipate that the preservation of equivariance to rotations and translations on spatial coordinates via the EGCN structure guarantees sufficient generalizability to various graph structures of dynamics systems. As a modified version of the graph convolutional network (Gilmer et al., 2017), an equivariant graph convolutional layer can be expressed by the following equations:

$$m_{ij} = \phi_e(h_i^{(l)}, h_j^{(l)}, ||x_i^{(l)} - x_j^{(l)}||^2, a_{ij}) \tag{7}$$

$$x_i^{(l+1)} = x_i^{(l)} + C \sum_{j \neq i} (x_i^{(l)} - x_j^{(l)})\phi_x(m_{ij}) \tag{8}$$

$$m_i = x_i^{(l)} + C \sum_{j \neq i} m_{ij} \tag{9}$$

$$h_i^{(l+1)} = \phi_h(h_i^{(l)}, m_i) \tag{10}$$

where a_{ij} is the edge attributes, x_i and x_j are the 2D coordinate embeddings for node i and j, respectively, and C is a constant for normalization computed as $1/|\mathcal{N}(i)|$. For the edge attributes, we use five attributes that can be extracted from the connecting nodes: distance, surface slope, base slope, and gradient of the x and y components of the ice velocity. ϕ_e, ϕ_x, and ϕ_h are the edge, position, and node operations, respectively, which are approximated by single-layer MLPs. The translation and rotation
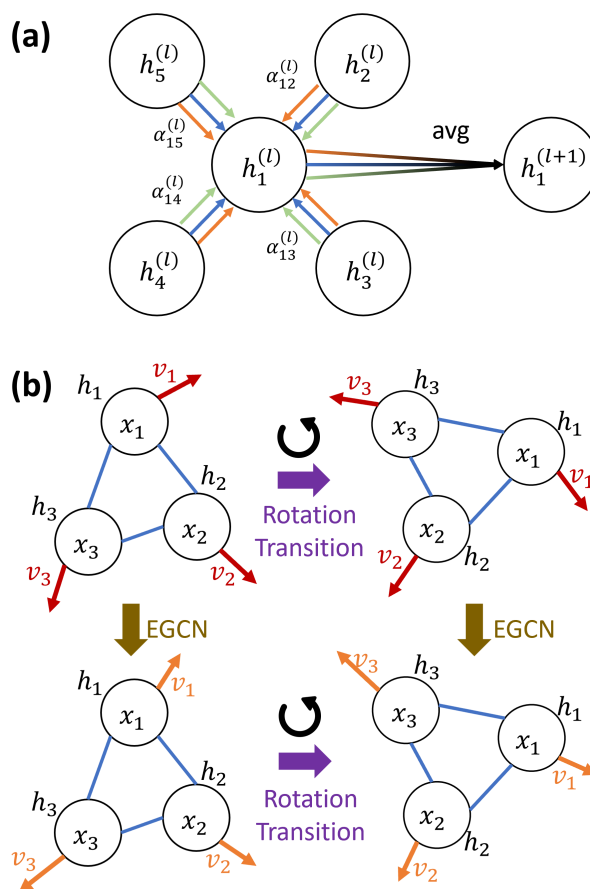
Figure 3. (a) Illustration of attention mechanism of GAT (Veličković et al., 2018). The node feature at lth layer $h_1^{(l)}$ is updated to $h_1^{(l+1)}$ from the three attention scores from each neighboring node. The average of the 3 attention mechanisms become $h_1^{(l+1)}$; (b) Concept of equivariance to rotation and transition of EGCN (Satorras et al., 2022).

equivariance can be preserved through Equation 8 (Satorras et al., 2022). Herein, we regard the x- and y-components of the ice velocity as the displacement causing coordinate change of the nodes of the graph, even though the graph structure itself remains

220   unchanged over time. Thus, in the EGCN, among the four output variables, the x- and y-components of the ice velocity are represented as the coordinate embeddings $x_i^{(l)}$ in Eq. 8 and 9, and ice thickness and ice mask are represented by $h_i^{(l)}$. Thus, the ice thickness and ice mask features are equivariant to the displacement caused by ice flow. Additionally, this equivariant operation is flexible since the embedding message m_{ij} can carry information from the entire graph and not only from the specific neighboring nodes (Satorras et al., 2022). Similar to the GCN and GAT, the EGCN also consists of one input layer, five

225   equivariant graph convolutional layers with 128 features, and one output layer (Fig. 2).

4.4   Convolutional Neural Network

As a baseline, or "control" model to compare our GNN emulators against, we train and test a fully convolutional network (FCN), which has a similar architecture as the one described in Jouvet et al. (2022). Our FCN architecture consists of 5 hidden convolutional layers, and each convolution has a 3×3 kernel size and 128 features. The leaky ReLU activation function of

230   0.01 negative slope is applied after each convolutional layer. Since the FCN takes regular grids as the input and output, the interpolated 200 m grid datasets are used as the input and output of the FCN, but the output of the FCN is interpolated onto the original triangular mesh for comparison.

4.5   Model training

From the ice sheet simulation results, we collect 2,349 graph structures (261 sets of results per transient simulations × 9 $\sigma_{\max}$

235   values). Our GNN takes 8 features of those graph nodes as inputs, including time t, $\sigma_{\max}$, bed elevation, surface mass balance (SMB), initial ice thickness, x and y components of the ice velocity at time $t-1$, and ice mask at time $t-1$. Then, after forwarding processes, the output layer predicts 4 features of those graph nodes at time t: the two components of the ice velocity, ice thickness, and ice mask (Fig. 2). All input and output features are normalized to the range [-1, 1] for stable learning using the nominal maximum and minimum values of these variables.

240   All 2,349 graph structures are divided into training, validation, and test datasets based on the $\sigma_{\max}$ values to assess if our emulators can be generalized for out-of-sample $\sigma_{\max}$ values. The data with $\sigma_{\max}$ equal to 0.70, 0.80, 0.85, 0.90, 1.00, 1.05, and 1.10 MPa are used for training and validation: we randomly split them into 70% and 30% for training and testing, respectively. The remaining data, with $\sigma_{\max}$ equal to 0.75 and 0.95 MPa, are used as test datasets. Consequently, the number of training, validation, and test graph datasets is 1279, 548, and 522, respectively. The model is optimized by Adam stochastic gradient

245   descent algorithm with the mean square error (MSE) loss function, over 500 epochs, and a learning rate of 0.001.

4.6   Model evaluation

We evaluate the ability of our emulators to reproduce ice velocity, ice thickness, and calving front migration by comparing them to ISSM simulation results. For this evaluation, we calculate three metrics: (i) root mean square error (RMSE), (ii) correlation

11

coefficient (R), and (iii) binary accuracy score (BiAcc); RMSE and R are used to evaluate ice velocity and ice thickness
250   predictions, and BiAcc is used to evaluate the calving front delineation. These metrics are calculated using the following
equations:

$$\text{RMSE}(\hat{y}, y) = \sqrt{\frac{1}{N}\sum_{i=1}^{N}(\hat{y}_i - y_i)^2} \tag{11}$$

$$R(\hat{y}, y) = \frac{\sum^{i}(\hat{y}_i - \bar{\hat{y}})(y_i - \bar{y})}{\sqrt{\sum^{i}(\hat{y}_i - \bar{\hat{y}})^2 \sum^{i}(y_i - \bar{y})^2}} \tag{12}$$

255

$$\text{BiAcc}(\hat{y}, y) = \frac{1}{N}\sum_{i=1}^{N}\mathbf{I}(\hat{y}_i = y_i) \tag{13}$$

where $\hat{y}$ denotes predicted values, y denotes true values, N is the number of data points, and $\mathbf{I}(\hat{y}_i = y_i)$ denotes the indication
function that returns 1 if $\hat{y}_i = y_i$ and returns 0 if $\hat{y}_i \neq y_i$. RMSE represents the difference between the prediction and reference;
lower RMSE corresponds to better fidelity. R represents the spatial correlation between the prediction and reference, ranging
260   from -1 to 1; R close to 1 means that the prediction agrees with the "ground truth" more. In calculating BiAcc, we convert the
ice mask into binary values, representing ice nodes as 1 and non-ice nodes as 0. Therefore, BiAcc is a metric indicating the
proportion of accurately predicted nodes relative to the total number of nodes.

5   Results

In this study, we apply the GNN and FCN emulators to predict changes in ice sheet dynamics and ice front position of Helheim
265   Glacier. We evaluate the model accuracy and computational efficiency of these emulators and examine the effect of the tunable
parameter σ_{max} on the ability of the model to match observations.

5.1   Model Fidelity

Our GNN models are trained with seven σ_{max} values of 0.70, 0.80, 0.85, 0.90, 1.00, 1.05, and 1.10 MPa, and these trained
models are tested with two out-of-sample σ_{max} values of 0.75 and 0.95 MPa. Table 1 displays the accuracy in ice velocity, ice
270   thickness, and calving front position for deep learning emulators at the test σ_{max} values. Overall, all deep learning emulators
exhibit remarkable performance in predicting ice velocity and thickness, with R-values greater than 0.997. Moreover, as depicted
in Fig. 4 and 5, all emulators successfully reproduce the retreat of ice front at lower σ_{max} and the advance of ice front at higher
σ_{max}. However, the deep learning emulators show lower accuracy at lower σ_{max} (0.75 MPa), which corresponds to a higher
chance of calving and more dynamic ice flow conditions. The sudden changes in ice dynamics and calving under a lower σ_{max}

275 values could make it challenging for the GNN emulators to replicate the exact results of the numerical model. On the other hand, since the ice front remains relatively stable at a higher σ_{max} value, it could be easier to predict this stable state of the glacier at 0.95 MPa of σ_{max}.

Table 1. Accuracy of ice velocity, ice thickness, and ice front position retrieved from the GCN, GAT, EGCN, and FCN surrogate models on two test σ_{max} values.

Model	σ_{max} (MPa)	Ice velocity		Ice thickness		Calving front
		RMSE (m/year)	R	RMSE (m)	R	Acc (%)
FCN	0.75	123.36	0.997	41.88	0.996	98.6
	0.95	118.60	0.997	40.55	0.996	98.6
	Average	120.98	0.997	41.22	0.996	98.6
GCN	0.75	88.35	0.998	37.57	0.997	98.4
	0.95	77.10	0.999	35.81	0.997	99.2
	Average	82.73	0.998	36.69	0.997	98.8
GAT	0.75	77.09	0.999	37.90	0.997	99.1
	0.95	71.06	0.999	34.94	0.997	99.1
	Average	74.08	0.999	36.42	0.997	99.1
EGCN	0.75	42.43	0.999	30.82	0.998	99.5
	0.95	39.24	0.999	27.60	0.998	99.4
	Average	**40.84**	**0.999**	**29.21**	**0.998**	**99.4**

In terms of ice velocity, all three GNN models demonstrate better accuracy than the FCN for both σ_{max} values. As shown in the ice velocity maps in Fig. 4, the FCN exhibits higher errors, particularly along the boundary between fast and slow ice in the 280 main ice stream. These large errors around the edge of the ice stream can be attributed to the fixed resolution and connectivity of the FCN. While ISSM uses a finer mesh resolution for fast ice regions to capture detailed ice dynamics, the FCN uses a uniform 200 m resolution grid across the entire domain. Hence, the FCN struggles to accurately describe the detailed ice dynamics in regions of sharp gradients, such as shear margins. On the other hand, GNNs can fully leverage the adaptive meshes of the ISSM by using the original mesh and connecting information between nodes. Among the three GNN emulators, the EGCN 285 shows the best accuracy, followed by GAT and GCN. In general, EGCN reduces the RMSE of ice velocity by 30-40 m/year compared to the other GNN architectures. As mentioned in section 4, the GCN, GAT, and EGCN have distinct characteristics in message-passing approaches: the GCN simply uses the adjacency status between neighboring nodes to determine the weights during the propagation process (Eq. 3); the GAT uses additional self-attention mechanisms to evaluate the relative importance of neighboring nodes (Eq. 5); the EGCN uses the message passing from all nodes to preserve the equivariance of the entire graph

290 (Eq. 7 and 8). We conjecture that the equivariance architecture of the EGCN contributes significantly to the improvement of model fidelity.

In terms of ice thickness, the EGCN also shows the best accuracy, with an average RMSE of 29.21 m (Table 1) and notably lower errors across the entire model domain (Fig. 5). The GCN and GAT have similar RMSEs of around 36 m for ice thickness prediction, while the FCN still has the largest RMSE of > 40 m. Similar to the ice velocity results, the FCN shows larger errors 295 near the boundary of the ice stream due to its limited resolution and node connectivity (Fig. 5).

The best fidelity from the EGCN and the worst fidelity from the FCN are also observed for the calving front position prediction (Table 1). The BiAcc of the FCN averages around $\sim$98.6%, whereas that of the EGCN reaches 99.4%. This supports the notion that the equivariance concept of the EGCN is beneficial in predicting the dynamic movement of the ice front. The location of the ice front at the end of the transient simulation for different σ_{max} values, retrieved from ISSM and deep learning emulators, are 300 shown in Fig. 6. All emulators predict the retreat of the ice front at lower σ_{max} values and the advance of the ice front at higher σ_{max} values, which agrees with the results of ISSM. It is noteworthy that the calving front prediction of the EGCN agrees best with the ISSM.

5.2 Computational time

The most significant advantage of GNN emulators is their ability to reduce computation time dramatically by leveraging GPUs. 305 We record and compare the time required to generate the final transient simulations for seven different σ_{max} values using ISSM and our GNN emulators (Table 2). The computation time of ISSM represents the total elapsed time spent on a single node of the Texas Advanced Computing Center (TACC) Frontera supercomputing cluster, which is equipped with 56 cores of Intel 8280 Cascade Lake CPUs (192 GB memory). The computation times of GNN emulators represent the total elapsed time on a CPU (Intel(R) Core(TM) i7-11700F; 32 GB memory) and GPU (NVIDIA GeForce RTX 3070; 24GB memory) of the same desktop 310 (Lenovo Legion T5 26IOB6). We observe a dramatic speed-up with GPU-based deep learning emulators, achieving computation times that are 250-560 times faster than ISSM simulations. Specifically, the GCN shows the highest speed-up, around 560 times faster than ISSM, and the FCN shows the least speed-up, being around 250 times faster. It is also noteworthy that using GPUs reduces the computation time of deep learning emulators by 16-37 times compared to using CPUs.

This experiment is also promising because, while ISSM computation is performed on a supercomputer, GNNs can be run on a 315 personal desktop. By using GPU-based GNN emulators, the computationally intensive solutions of ice dynamics and calving can be quickly reproduced on personal desktops without the need for high-performance computing systems. We expect that these types of emulators will facilitate the effective parameterization of different ice conditions, ice properties, and external climate forcings.

However, although GNNs can successfully replicate the finite-element structure of ISSM simulations and reduce the 320 computational time by leveraging GPUs, it is important to consider the upstream costs for training deep learning emulators to assess their whole-process efficiencies. Table 3 shows the number of learnable parameters and model training time for FCN, GCN, GAT, and EGCN. This training time is recorded from the 500-epoch training of each model on a multiple-GPU system equipped with 8 NVIDIA RTX A5000 GPUs. GCN takes the least training time, followed by GAT, EGCN, and FCN. FCN

14
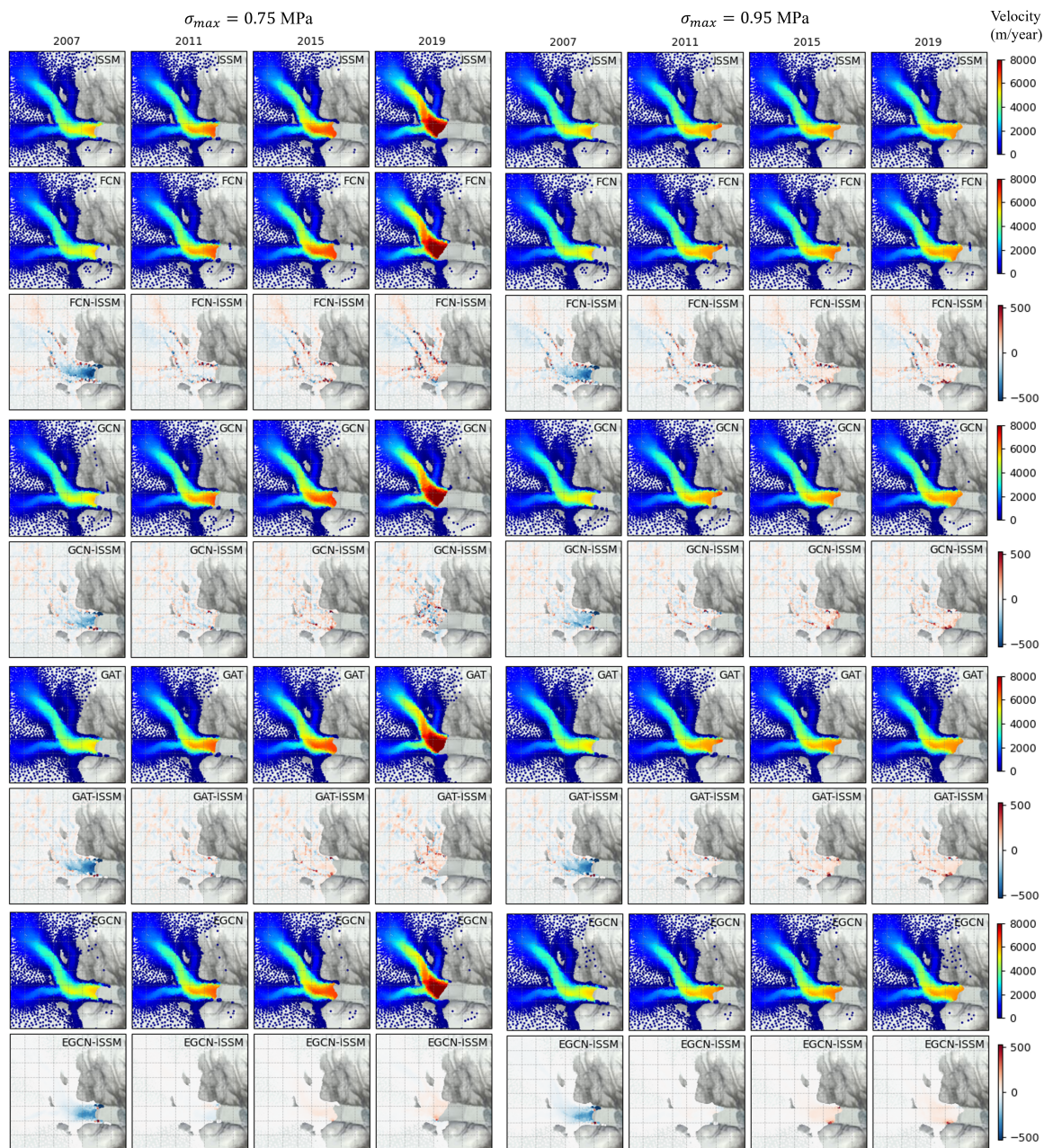
Figure 4. Maps of ISSM-simulated ice velocity, FCN-emulated ice velocity and difference with ISSM, GCN-emulated ice velocity and difference with ISSM, GAT-emulated ice velocity and difference with ISSM, and EGCN-emulated ice velocity and difference with ISSM (from top to bottom) for 0.75 MPa and 0.95 MPa of calving thresholds $\sigma_{\max}$.
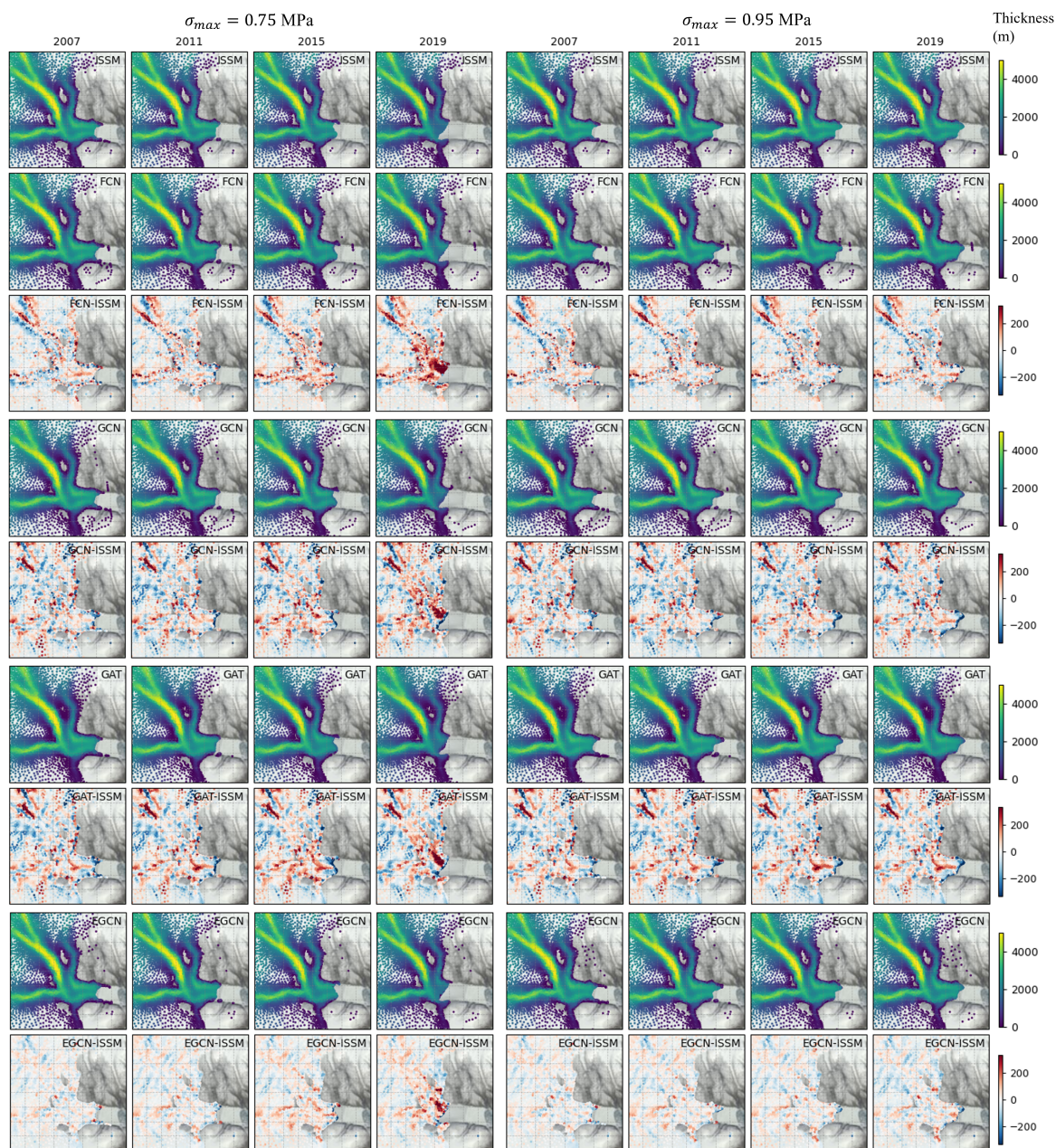
Figure 5. ISSM-simulated ice thickness, FCN-emulated ice thickness and difference with ISSM, GCN-emulated ice thickness and difference with ISSM, GAT-emulated ice thickness and difference with ISSM, and EGCN-emulated ice thickness and difference with ISSM (from top to bottom) for 0.75 MPa and 0.95 MPa of calving thresholds $\sigma_{\max}$.
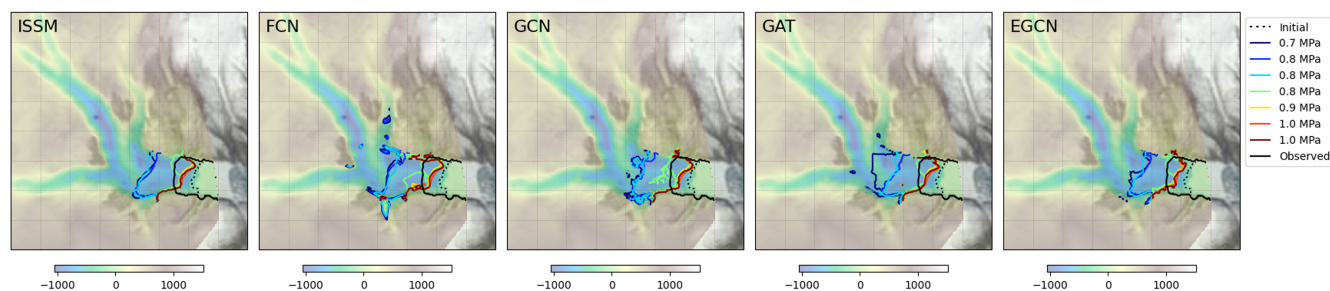
Figure 6. Calving front in 2020 for different $\sigma_{\max}$ predicted by ISSM and deep learning emulators.

takes around 11.8 times, 5.3 times, and 4.5 times more training time than GCN, GAT, and EGCN, respectively. It is noted
325   that FCN shows inferior accuracy compared to the others despite its longer training time. Therefore, considering upstream
computational time, post-training computation time, and fidelity of the model, GNN architectures appear to be more efficient
tools than traditional CNNs for emulating finite-element ice sheet dynamics. Moreover, given that improving resolution in a
regular grid of CNN requires exponentially increasing computations, the irregular graph structures would be more practical if
high-resolution information is required.

Table 2. Computation time (seconds) for generating the 13-year transient results from ISSM and GNN emulators

METHOD	MODEL	CPU	GPU
NUMERICAL	ISSM	6681.25	-
EMULATOR	GCN	200.58	**11.89**
	GAT	772.66	20.88
	EGCN	759.37	25.42
	FCN	851.71	27.01

Table 3. Upstream computational time for training deep learning models

Model	Number of learnable parameters	Training time (seconds)
FCN	604,292	4151.49
GCN	67,843	349.45
GAT	205,656	772.31
EGCN	269,826	906.71

5.3 Comparison with real observations

330

We use these GNN emulators to determine the appropriate range of σ_{max} values to accurately capture the migration of Helheim's calving front. The satellite-derived ice velocity and ice front observations at each time step are used as input for the GNN models to predict the ice front at the next time step. Then, we identify the optimal σ_{max} value for each time step that maximizes the BiAcc of ice front location between prediction and observation (Eq. 13). Given that previous studies (Morlighem et al., 2016; Wilner et al., 2023; Choi et al., 2018) suggest that σ_{max} should fall between 0.7 to 1.1 MPa, we vary σ_{max} incrementally by 0.01 MPa within this range and determine the σ_{max} value with the highest BiAcc. Fig. 7a-c shows the range of σ_{max} with > 95 % of accuracy, derived from the three GNN emulators spanning 2007 to 2020. Although the GCN (Fig. 7a) exhibits a different trend in the first 2 years (2007-2008) compared to the GAT (Fig. 7b) and EGCN (Fig. 7c), the optimal σ_{max} generally increases after 2009 for all emulators. These results indicate that the early years have a relatively wide range of > 95 % accuracy σ_{max}

335

340

compared to the late few years. While the best σ_{max} appears to be around 0.8±0.15 MPa in 2009, this range shifts to around 1.0±0.07 MPa after 2016. The GNN emulators enable us to determine the appropriate σ_{max} range almost 260-600 times faster than traditional numerical models. While this parameter search process is laborious and time-consuming with numerical models, it is relatively quick and simple with GNNs; we determine this effective range by simply replacing the input variables of the deep learning models with real observations.

In order to understand the scientific implication of this σ_{max} variation, we also examine the calving front and ice velocity from satellite observations for two flow lines (Fig. 1b). In the early years before 2014, the ice front remains relatively stable (with < 2 km of retreat/advance) without significant advances or retreats (Fig. 7d and e). However, after 2014, the ice front moves more dynamically: ice front retreat reaches up to 4 km in the summers of 2017 and 2019 (Fig. 7d and e). Considering that σ_{max} increases from 2009-2014 and remains consistently at 1.0±0.7 MPa after 2014, we suggest that additional environmental factors

345

350

(e.g., mélange or ocean thermal forcing) could have contributed to changes in calving rates after 2014. Although this study only investigates the sensitivity of modeled ice front position to the calving threshold σ_{max} based on VM, GNN emulators can be further utilized to investigate the impact of any other model input, such as external forcings.

6 Discussion

The results of this study demonstrate the superiority of GNN architectures, especially EGCN, over traditional CNN architectures

355

in emulating numerical ice sheet models operating on unstructured meshes. Firstly, in terms of model fidelity, traditional CNN architectures require the interpolation of the unstructured meshes into rectangular meshes, resulting in a loss of accuracy, especially in the regions with high resolution on the original unstructured mesh. Using GNN directly on raw unstructured meshes keeps high resolution in fast ice regions that significantly affect the dynamics of the entire ice sheet domain. In particular, EGCN shows the best fidelity in predicting ice thickness due to its equivariance concept throughout the graph structures. Secondly,

360

GNN architectures can preserve the computational efficiency inherent to unstructured meshes. ISSM allocates computational resources by assigning finer resolution to fast flow regions and coarser resolution to slow moving regions. However, using rectangular meshes and CNN disrupts this efficient allocation, eventually increasing the computation time. Indeed, as shown in
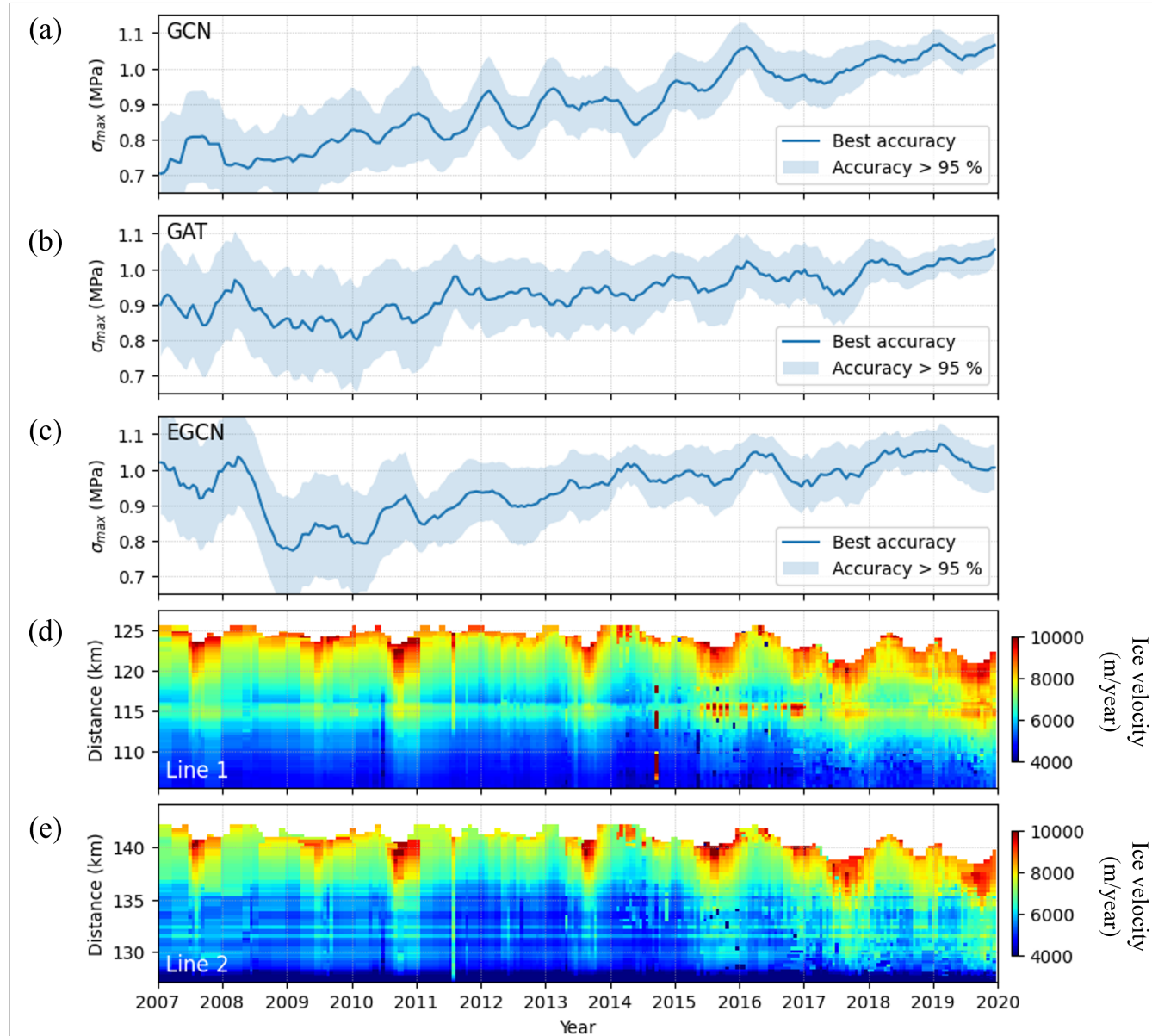
Figure 7. Optimal $\sigma_{\max}$ compared with the real observations .

section 5.2, FCN requires 4-12 times longer training time compared to GNN emulators. If we use a rectangular grid with a finer resolution than 1 km, CNN will take a longer time due to the inefficient allocation of too-fine resolutions for where ice flow is
365 slow.

Moreover, GNN emulators have significant potential for further improvement, particularly through integration with various architectures, including recurrent neural networks (RNNs) and attention mechanisms (Wu et al., 2021). For example, embedding recurrent units into the GNN architecture would make it possible to find the sequential relationships between ice sheet dynamics and calving parameters. This recurrent GNN architecture will be able to predict how the historical context of calving parameters
370 affects ice dynamics and ice front migration. As the pioneering study to evaluate the potential of GNN for connecting calving parameterizations and ice sheet dynamics, this research provides insights into how GNN can be effectively utilized in glaciology.

Nevertheless, it is also worth noting several limitations of our approach. Firstly, despite the computational efficiency of GNN emulators, they should be trained using numerical simulations. Since the model performance is highly dependent on the quality of training datasets, simulation data should be collected carefully with appropriate parameterizations. Additionally, the collection
375 of training datasets from various climatological scenarios is essential for better generalizability and reliability of emulators; however, this process can be exceptionally time-consuming. Secondly, although we use numerical simulation data based on the VM calving law for training, it is important to recognize that calving mechanisms are not yet fully understood and may be more complex than those represented by the VM law. While the VM method has been validated for many glaciers in Greenland and Antarctica (Choi et al., 2018; Wilner et al., 2023), detailed calving mechanisms remain elusive. Thus, although our GNN
380 emulators provide valuable insights into calving mechanisms based on VM calving law, they cannot provide implicit solutions for all calving processes.

7   Conclusions

This study develops three standard graph neural networks: graph convolutional network, graph attention network, and equivariant graph convolutional network, as surrogate models to reproduce finite-element ice dynamics and calving retrieved from the ISSM.
385 After training these GNNs with the 13-year transient simulation results from Helheim Glacier, they demonstrate significant spatiotemporal agreement with ISSM simulations in predicting ice velocity, ice thickness, and ice front location. Additionally, the GNN emulators successfully reproduce the retreat of the ice front for a lower calving stress threshold σ_{max}, as well as the stable condition of the ice front for a higher σ_{max}. Among the three GNN architectures, the EGCN shows the best robustness by preserving the equivariance of graph structures regardless of displacement caused by ice movement. Given that
390 our GNN emulators can reduce computational time by 260-560 times, even on a personal desktop, they are a promising tool for investigating the impact of parameterizations on future ice sheet behavior. By simply applying satellite-derived observations to these computationally efficient GNNs, we find that the optimal σ_{max} of the von Mises calving law should slightly increase from 2007 to 2020 for Helheim Glacier. This study represents the first attempt to use GNNs for modeling ice sheet dynamics and calving, ultimately contributing to improving the prediction accuracy of ice sheet mass loss and resulting sea level rise under
395 rapidly changing climate conditions.

Code and data availability. All the code and data are available through this link: https://github.com/BinaLab/ISSM_GNN and https://zenodo.org/records/11392220

400

Competing interests. GC is a member of the editorial board of The Cryosphere. All other authors declare that they have no conflict of interest.

References

405   Aschwanden, A., Fahnestock, M. A., Truffer, M., Brinkerhoff, D. J., Hock, R., Khroulev, C., Mottram, R., and Khan, S. A.: Contribution of the Greenland Ice Sheet to sea level over the next millennium, Science Advances, 5, eaav9396, https://doi.org/10.1126/sciadv.aav9396, 2019.

Bevan, S. L., Luckman, A., Khan, S. A., and Murray, T.: Seasonal dynamic thinning at Helheim Glacier, Earth and Planetary Science Letters, 415, 47–53, 2015.

Black, N. and Najafi, A. R.: Learning finite element convergence with the multi-fidelity graph neural network, Computer Methods in Applied 410   Mechanics and Engineering, 397, 115 120, 2022.

Bondzio, J., Morlighem, M., Seroussi, H., Kleiner, T., Ruckamp, M., Mouginot, J., Moon, T., Larour, E., and Humbert, A.: The mechanisms behind Jakobshavn Isbræ's acceleration and mass loss: A 3-D thermomechanical model study, Geophys. Res. Lett., 44, https://doi.org/10.1002/2017GL073309, 2017.

Bondzio, J. H., Seroussi, H., Morlighem, M., Kleiner, T., Rückamp, M., Humbert, A., and Larour, E. Y.: Modelling calving front dynamics using 415   a level-set method: application to Jakobshavn Isbræ, West Greenland, The Cryosphere, 10, 497–510, https://doi.org/10.5194/tc-10-497-2016, 2016.

Cheng, G., Morlighem, M., Mouginot, J., and Cheng, D.: Helheim Glacier's Terminus Position Controls Its Seasonal and Inter-Annual Ice Flow Variability, Geophysical Research Letters, 49, e2021GL097 085, 2022.

Choi, Y., Morlighem, M., Wood, M., and Bondzio, J. H.: Comparison of four calving laws to model Greenland outlet glaciers, The Cryosphere, 420   12, 3735–3746, https://doi.org/10.5194/tc-12-3735-2018, 2018.

Choi, Y., Morlighem, M., Rignot, E., and Wood, M.: Ice dynamics will remain a primary driver of Greenland ice sheet mass loss over the next century, Communications Earth & Environment, 2, 26, 2021.

Choi, Y., Seroussi, H., Morlighem, M., Schlegel, N.-J., and Gardner, A.: Impact of time-dependent data assimilation on ice flow model initialization and projections: a case study of Kjer Glacier, Greenland, The Cryosphere, 17, 5499–5517, https://doi.org/10.5194/tc-17-5499- 425   2023, 2023.

dos Santos, T. D., Morlighem, M., and Seroussi, H.: Assessment of numerical schemes for transient, finite-element ice flow models using ISSM v4.18, Geoscientific Model Development, 14, 2545–2573, https://doi.org/10.5194/gmd-14-2545-2021, 2021.

Downs, J., Brinkerhoff, D., and Morlighem, M.: Inferring time-dependent calving dynamics at Helheim Glacier, Journal of Glaciology, 69, 381–396, https://doi.org/10.1017/jog.2022.68, 2023.

430   Edwards, T., Nowicki, S., Goelzer, H., Seroussi, H., Marzeion, B., Smith, C. E., Jourdain, N. C., Slater, D., McKenna, C., Simon, E., Abe-Ouchi, A., Gregory, J., Hock, R., Larour, E., Lipscomb, W., Payne, A., Shepherd, A., Agosta, C., Alexander, P., Albrecht, T., Anderson, B., Asay-Davis, X., Aschwanden, A., Barthel, A., Calov, R., Chambers, C., Golledge, N., Greve, R., Hatterman, T., Hoffman, M., Humbert, A., Huss, M., Huybrechts, P., Immerzeel, W., Kleiner, T., Kraaijenbrink, P., Le Clec'h, S., Lee, V., Leguy, G., Little, C., Lowry, D., Malles, J.-H., Maussion, F., Morlighem, M., Nias, I., Pattyn, F., Pelle, T., Price, S., Quiquet, A., Radic, V., Reese, R., Rounce, D., Rückamp, M., Sakai, A., 435   Schlegel, N., Trusel, L. D., Van Breedam, J., Van De Wal, R. S. W., van den Broeke, M., Winkelmann, R., Zhao, C., Zhang, T., Zekollari, H., Zwinger, T., Champollion, N., Choi, Y., Cullather, R., Cuzzone, J., Dumas, C., Felikson, D., Fettweis, X., Fujita, S., and Gladstone, R.: Quantifying uncertainties in the land ice contribution to sea level rise this century, Nature, 593, https://doi.org/10.1038/s41586-021-03302-y, 2021.

Fu, X., Zhou, F., Peddireddy, D., Kang, Z., Jun, M. B.-G., and Aggarwal, V.: An finite element analysis surrogate model with boundary 440   oriented graph embedding approach for rapid design, Journal of Computational Design and Engineering, 10, 1026–1046, 2023.

Gagliardini, O., Zwinger, T., Gillet-Chaulet, F., Durand, G., Favier, L., de Fleurian, B., Greve, R., Malinen, M., Martín, C., Råback, P., Ruokolainen, J., Sacchettini, M., Schäfer, M., Seddik, H., and Thies, J.: Capabilities and performance of Elmer/Ice, a new-generation ice sheet model, Geoscientific Model Development, 6, 1299–1318, https://doi.org/10.5194/gmd-6-1299-2013, 2013.

Gilmer, J., Schoenholz, S. S., Riley, P. F., Vinyals, O., and Dahl, G. E.: Neural Message Passing for Quantum Chemistry, 2017.

445 Greene, C. A., Gardner, A. S., Wood, M., and Cuzzone, J. K.: Ubiquitous acceleration in Greenland Ice Sheet calving from 1985 to 2022, NATURE, 625, https://doi.org/10.1038/s41586-023-06863-2, 2024a.

Greene, C. A., Gardner, A. S., Wood, M., and Cuzzone, J. K.: Ubiquitous acceleration in Greenland Ice Sheet calving from 1985 to 2022, Nature, 625, 523–528, 2024b.

He, Q., Perego, M., Howard, A. A., Karniadakis, G. E., and Stinis, P.: A hybrid deep neural operator/finite element method for ice-sheet 450 modeling, Journal of Computational Physics, 492, 112 428, https://doi.org/https://doi.org/10.1016/j.jcp.2023.112428, 2023.

Jiang, C. and Chen, N.-Z.: Graph Neural Networks (GNNs) based accelerated numerical simulation, Engineering Applications of Artificial Intelligence, 123, 106 370, 2023.

Jouvet, G.: Inversion of a Stokes glacier flow model emulated by deep learning, Journal of Glaciology, 69, 13–26, https://doi.org/10.1017/jog.2022.41, 2023.

455 Jouvet, G. and Cordonnier, G.: Ice-flow model emulator based on physics-informed deep learning, Journal of Glaciology, p. 1–15, https://doi.org/10.1017/jog.2023.73, 2023.

Jouvet, G., Picasso, M., Rappaz, J., and Blatter, H.: A new algorithm to simulate the dynamics of a glacier: theory and applications, Journal of Glaciology, 54, 801–811, https://doi.org/10.3189/002214308787780049, 2008.

Jouvet, G., Cordonnier, G., Kim, B., Lüthi, M., Vieli, A., and Aschwanden, A.: Deep learning speeds up ice flow modelling by several orders 460 of magnitude, Journal of Glaciology, 68, 651–664, https://doi.org/10.1017/jog.2021.120, 2022.

King, M. D., Howat, I. M., Candela, S. G., Noh, M. J., Jeong, S., Noël, B. P., van den Broeke, M. R., Wouters, B., and Negrete, A.: Dynamic ice loss from the Greenland Ice Sheet driven by sustained glacier retreat, Communications Earth & Environment, 1, 1, 2020.

Kipf, T. N. and Welling, M.: Semi-Supervised Classification with Graph Convolutional Networks, https://doi.org/10.48550/arXiv.1609.02907, 2017.

465 Larour, E., Seroussi, H., Morlighem, M., and Rignot, E.: Continental scale, high order, high spatial resolution, ice sheet modeling using the Ice Sheet System Model (ISSM), Journal of Geophysical Research: Earth Surface, 117, https://doi.org/https://doi.org/10.1029/2011JF002140, 2012.

Lippert, E., Morlighem, M., Cheng, G., and Khan, S.: Modeling a century of change: Kangerlussuaq Glacier's mass loss from 1933 to 2021, Geophysical Research Letters, 51, e2023GL106 286, 2024.

470 MacAyeal, D. R.: Large-scale ice flow over a viscous basal sediment: Theory and application to ice stream B, Antarctica, Journal of Geophysical Research: Solid Earth, 94, 4071–4087, https://doi.org/https://doi.org/10.1029/JB094iB04p04071, 1989.

Maurizi, M., Gao, C., and Berto, F.: Predicting stress, strain and deformation fields in materials and structures with graph neural networks, Scientific Reports, 12, 21 834, 2022.

Miles, V. V., Miles, M. W., and Johannessen, O. M.: Satellite archives reveal abrupt changes in behavior of Helheim Glacier, southeast 475 Greenland, Journal of Glaciology, 62, 137–146, 2016.

Morlighem, M., Bondzio, J., Seroussi, H., Rignot, E., Larour, E., Humbert, A., and Rebuffi, S.: Modeling of Store Gletscher's calving dynamics, West Greenland, in response to ocean thermal forcing, Geophysical Research Letters, 43, 2659–2666, https://doi.org/https://doi.org/10.1002/2016GL067695, 2016.

Morlighem, M., Williams, C. N., Rignot, E., An, L., Arndt, J. E., Bamber, J. L., Catania, G., Chauché, N., Dowdeswell, J. A., Dorschel,
480   B., Fenty, I., Hogan, K., Howat, I., Hubbard, A., Jakobsson, M., Jordan, T. M., Kjeldsen, K. K., Millan, R., Mayer, L., Mouginot, J.,
        Noël, B. P. Y., O'Cofaigh, C., Palmer, S., Rysgaard, S., Seroussi, H., Siegert, M. J., Slabon, P., Straneo, F., van den Broeke, M. R.,
        Weinrebe, W., Wood, M., and Zinglersen, K. B.: BedMachine v3: Complete Bed Topography and Ocean Bathymetry Mapping of
        Greenland From Multibeam Echo Sounding Combined With Mass Conservation, Geophysical Research Letters, 44, 11,051–11,061,
        https://doi.org/https://doi.org/10.1002/2017GL074954, 2017.

485   Morlighem, M., Rignot, E., Binder, T., Blankenship, D., Drews, R., Eagles, G., Eisen, O., Ferraccioli, F., Forsberg, R., Fretwell, P., Goel,
        V., Greenbaum, J. S., Gudmundsson, H., Guo, J., Helm, V., Hofstede, C., Howat, I., Humbert, A., Jokat, W., Karlsson, N. B., Lee, W. S.,
        Matsuoka, K., Millan, R., Mouginot, J., Paden, J., Pattyn, F., Roberts, J., Rosier, S., Ruppel, A., Seroussi, H., Smith, E. C., Steinhage, D.,
        Sun, B., Broeke, M. R. v. d., Ommen, T. D. v., Wessem, M. v., and Young, D. A.: Deep glacial troughs and stabilizing ridges unveiled
        beneath the margins of the Antarctic ice sheet, Nat. Geosci., 13, 132–137, https://doi.org/10.1038/s41561-019-0510-8, 2020.

490   Mouginot, J., Rignot, E., Scheuchl, B., and Millan, R.: Comprehensive annual ice sheet velocity mapping using Landsat-8, Sentinel-1, and
        RADARSAT-2 data, Remote Sensing, 9, 364, 2017.

        Mouginot, J., Rignot, E., Bjørk, A. A., van den Broeke, M., Millan, R., Morlighem, M., Noël, B., Scheuchl, B., and Wood, M.: Forty-six
        years of Greenland Ice Sheet mass balance from 1972 to 2018, Proceedings of the National Academy of Sciences, 116, 9239–9244,
        https://doi.org/10.1073/pnas.1904242116, 2019.

495   Osher, S. and Sethian, J. A.: Fronts propagating with curvature-dependent speed: Algorithms based on Hamilton-Jacobi formulations, Journal
        of Computational Physics, 79, 12–49, https://doi.org/https://doi.org/10.1016/0021-9991(88)90002-2, 1988.

        Otosaka, I. N., Shepherd, A., Ivins, E. R., Schlegel, N.-J., Amory, C., van den Broeke, M. R., Horwath, M., Joughin, I., King, M. D., Krinner,
        G., Nowicki, S., Payne, A. J., Rignot, E., Scambos, T., Simon, K. M., Smith, B. E., Sørensen, L. S., Velicogna, I., Whitehouse, P. L., A, G.,
        Agosta, C., Ahlstrøm, A. P., Blazquez, A., Colgan, W., Engdahl, M. E., Fettweis, X., Forsberg, R., Gallée, H., Gardner, A., Gilbert, L.,
500   Gourmelen, N., Groh, A., Gunter, B. C., Harig, C., Helm, V., Khan, S. A., Kittel, C., Konrad, H., Langen, P. L., Lecavalier, B. S., Liang,
        C.-C., Loomis, B. D., McMillan, M., Melini, D., Mernild, S. H., Mottram, R., Mouginot, J., Nilsson, J., Noël, B., Pattle, M. E., Peltier, W. R.,
        Pie, N., Roca, M., Sasgen, I., Save, H. V., Seo, K.-W., Scheuchl, B., Schrama, E. J. O., Schröder, L., Simonsen, S. B., Slater, T., Spada, G.,
        Sutterley, T. C., Vishwakarma, B. D., van Wessem, J. M., Wiese, D., van der Wal, W., and Wouters, B.: Mass balance of the Greenland and
        Antarctic ice sheets from 1992 to 2020, Earth System Science Data, 15, 1597–1616, https://doi.org/10.5194/essd-15-1597-2023, 2023.

505   Perera, R., Guzzetti, D., and Agrawal, V.: Graph neural networks for simulating crack coalescence and propagation in brittle materials,
        Computer Methods in Applied Mechanics and Engineering, 395, 115 021, https://doi.org/https://doi.org/10.1016/j.cma.2022.115021, 2022.

        Rignot, E., Xu, Y., Menemenlis, D., Mouginot, J., Scheuchl, B., Li, X., Morlighem, M., Seroussi, H., den Broeke, M. v., Fenty, I., et al.:
        Modeling of ocean-induced ice melt rates of five west Greenland glaciers over the past two decades, Geophysical Research Letters, 43,
        6374–6382, 2016.

510   Salehi, Y. and Giannacopoulos, D.: PhysGNN: A Physics–Driven Graph Neural Network Based Model for Predicting Soft Tissue Deformation
        in Image–Guided Neurosurgery, Advances in Neural Information Processing Systems, 35, 37 282–37 296, 2022.

        Satorras, V. G., Hoogeboom, E., and Welling, M.: E(n) Equivariant Graph Neural Networks, https://doi.org/10.48550/arXiv.2102.09844, 2022.

        Shivaditya, M. V., Alves, J., Bugiotti, F., and Magoulès, F.: Graph Neural Network-based Surrogate Models for Finite Element Analysis, in:
        2022 21st International Symposium on Distributed Computing and Applications for Business Engineering and Science (DCABES), pp.
515   54–57, IEEE, 2022.

Tedesco, M. and Fettweis, X.: Unprecedented atmospheric conditions (1948–2019) drive the 2019 exceptional melting season over the Greenland ice sheet, The Cryosphere, 14, 1209–1223, 2020.

Veličković, P., Cucurull, G., Casanova, A., Romero, A., Liò, P., and Bengio, Y.: Graph Attention Networks, https://doi.org/10.48550/arXiv.1710.10903, 2018.

520 Verjans, V. and Robel, A.: Accelerating Subglacial Hydrology for Ice Sheet Models With Deep Learning Methods, Geophysical Research Letters, 51, e2023GL105 281, https://doi.org/https://doi.org/10.1029/2023GL105281, e2023GL105281 2023GL105281, 2024.

Wilner, J. A., Morlighem, M., and Cheng, G.: Evaluation of four calving laws for Antarctic ice shelves, The Cryosphere, 17, 4889–4901, https://doi.org/10.5194/tc-17-4889-2023, 2023.

Winkelmann, R., Martin, M. A., Haseloff, M., Albrecht, T., Bueler, E., Khroulev, C., and Levermann, A.: The Potsdam Parallel Ice Sheet
525 Model (PISM-PIK) Part 1: Model description, The Cryosphere, 5, 715–726, https://doi.org/10.5194/tc-5-715-2011, 2011.

Wood, M., Rignot, E., Fenty, I., An, L., Bjørk, A., Broeke, M. v. d., Cai, C., Kane, E., Menemenlis, D., Millan, R., Morlighem, M., Mouginot, J., Noël, B., Scheuchl, B., Velicogna, I., Willis, J. K., and Zhang, H.: Ocean forcing drives glacier retreat in Greenland, Science Advances, 7, eaba7282, https://doi.org/10.1126/sciadv.aba7282, 2021.

Wu, Z., Pan, S., Chen, F., Long, G., Zhang, C., and Yu, P. S.: A Comprehensive Survey on Graph Neural Networks, IEEE Transactions on
530 Neural Networks and Learning Systems, 32, 4–24, https://doi.org/10.1109/TNNLS.2020.2978386, 2021.

Zhang, S., Tong, H., Xu, J., and Maciejewski, R.: Graph convolutional networks: a comprehensive review, Computational Social Networks, 6, 1–23, 2019.